Inorg. Chem. **2003**, *42*, 2253–2260

A New Quasi-One-Dimensional Ternary Chalcogenide: Synthesis, Crystal Structure, and Electronic Structure of $Nb_{1+x}V_{1-x}S_5$ ($x = 0.18$)

Hoseop Yun,*,† Geanha Ryu,† Stephen Lee,‡ and Roald Hoffmann‡

Department of Molecular Science and Technology, Ajou University, Suwon 442-749, Korea, and Department of Chemistry and Chemical Biology, Cornell University, Ithaca, New York 14853-1301

Received September 4, 2002

The new low-dimensional ternary chalcogenide, $Nb_{1+x}V_{1-x}S_5$ ($x = 0.18$), has been prepared and characterized. This compound crystallizes in the monoclinic space group, C_{2h}^2-$P2_1/m$ with two formula units in a cell with dimensions $a = 9.881(4)$ Å, $b = 3.329(1)$ Å, $c = 8.775(3)$ Å, and $\beta = 114.82(3)°$. The layer is composed of two unique chains of face-sharing Nb-centered bicapped trigonal prisms and edge-sharing M-centered octahedra (M = Nb or V). The electronic structures of the monomeric basic building units, NbS_8 and VS_6, and hypothetical and real one-, two-, and three-dimensional structures making up the compound are examined to understand the nature of inter- and intrachain interactions and orbital overlapping among metals and sulfur atoms. The electronic structure of $Nb_{1+x}V_{1-x}S_5$ is essentially given by superimposing those of the individual chains. V d orbitals are found to be crucial for the one-dimensional metallic conductivity along the chain axis.

Introduction

Group 5 metal chalcogenides are known for their low-dimensional crystal structures and interesting electronic properties, such as phase transitions involving the formation of charge density waves (CDW).[1] In $NbSe_3$ for example, two different CDW transitions have been observed, with onset temperatures of 144 and 59 K.[2] Attempts to dope $NbSe_3$ with other transition metals have led to a new layered phase of nominal composition $M_{1+x}Nb_{3-x}Se_{10}$ (M = Fe, Cr, V).[3] The compound, $Fe_{1+x}Nb_{3-x}Se_{10}$ ($x = 1/3$) has been the subject of numerous experimental and theoretical studies,[4] largely because its crystal and electronic structure have certain features in common with the well-known CDW material, $NbSe_3$. The structure of $Fe_{1+x}Nb_{3-x}Se_{10}$ consists of double $NbSe_6$ trigonal prismatic chains and double (Fe, Nb)Se_6 octahedral chains, both running parallel to the chain axis. The trigonal prismatic chains in $Fe_{1+x}Nb_{3-x}Se_{10}$ have interatomic distances and angles similar to those of one of the three types of chains found in $NbSe_3$. The Fe and Nb atoms on the octahedral chains, occurring in approximately a 2:1 ratio, are randomly distributed.[3] This Fe/Nb disorder, confined only to the octahedral chains, has been reported to be a crucial factor governing the transport properties.[4]

As pointed out by Cava et al.,[4c] one of the striking aspects of this phase is the limited extent to which it forms, along with its seeming to be only slightly more stable than the related binary phases. Attempts to substitute Nb in the octahedral site by other metals have not been successful, except for the inclusion of limited amounts of Fe, V, and Cr.[4c] In addition, no sulfide and telluride analogues of $Fe_{1+x}Nb_{3-x}Se_{10}$ are as yet known. Thus, studies on the relationship between structure and properties in this field have been hindered because of the lack of new materials.

As a side product of an attempt to synthesize new thiophosphates, $NbVPS_{10}$ or $CsNb_2PS_{10}$,[5] we were able to isolate

* Author to whom correspondence should be addressed. E-mail: hsyun@madang.ajou.ac.kr.

† Ajou University.

‡ Cornell University.

(1) (a) Whangbo, M. H. In *Crystal Chemistry and Properties of Materials with Quasi-One-Dimensional Structures*; Rouxel J., Ed.; D. Reidel Publishing Company: Dordrecht, Holland, 1986. (b) Rouxel, J. *J. Solid State Chem.* **1986**, *64*, 305−321.

(2) (a) Haen, P.; Monceau, P.; Tissier, B.; Waysand, G.; Meerschaut, A.; Molinie, P.; Rouxel, J. *Proc. Int. Conf. Low Temp. Phys., 14th* **1975**, 5, 445−448. (b) Ong, N. P.; Brill, J. W. *Phys. Rev.* **1978**, *B18* (10), 5265−5271.

(3) (a) Cava, R. J.; DiSalvo, F. J.; Eibschutz, M.; Waszczak, J. V. *Phys. Rev.* **1983**, *B27* (12), 7412−7419. (b) Gruber, H.; Bauer, E.; Sassik, H.; Steiner, W. *Physica* **1986**, *143B*, 204−206. (c) Salem, A. B.; Meerschaut, A.; Guemas, L.; Rouxel, J. *Mater. Res. Bull.* **1982**, *17*, 1071−1079.

(4) (a) Bullett, D. W. *J. Phys.* **1982**, *C15*, 3069−3077. (b) Evain, M.; Whangbo, M. H.; Salem, A. B.; Meerschaut, A. *Solid State Commun.* **1989**, *72* (10), 971−975. (c) Whangbo, M. H.; Cava, R. J.; DiSalvo, F. J.; Fleming, R. M. *Solid State Commun.* **1982**, *43* (4), 277−282.

10.1021/ic0205334 CCC: $25.00
Published on Web 03/12/2003

a new sulfide analogue of $Fe_{1+x}Nb_{3-x}Se_{10}$ as a minor product. Here we report the synthesis, crystal structure, and electronic structure of a new ternary sulfide, $Nb_{1+x}V_{1-x}S_5$ ($x = 0.18$).

Experimental Section

Synthesis. The compound $Nb_{1+x}V_{1-x}S_5$ was prepared by the reaction of elemental Nb, V, P, and S with the use of the reactive flux technique. A combination of the pure elements, Nb powder (CERAC 99.8%), V powder (CERAC 99.5%), P powder (CERAC 99.5%), and S powder (Aldrich 99.999%), was loaded in a quartz tube in an atomic ratio of Nb:V:P:S = 1:2:2:20, and then a CsCl/LiCl eutectic mixture was added in a weight ratio of $NbV_2P_2S_{20}$:CsCl/LiCl = 1:3. The tube was evacuated to $\sim 10^{-2}$ Torr, sealed, and heated gradually (80 °C/h) to 700 °C in a tube furnace, where it was kept for 7 days. The tube was slowly cooled to 200 °C at 4 °C /h and quenched. The excess halide was removed with distilled water.

Black shiny needle-shaped crystals up to 0.40 mm in length and dark-red needle-shaped crystals were found. Both crystals are stable in air and water. The dark-red crystals are the major phase and proved to be $CsNb_2PS_{10}$. A microprobe analysis of the black shiny needle-shaped crystals was made with an EDAX (Thermonoran) equipped scanning electron microscope (JEOL JXA-8900R). Analysis of these crystals showed only the presence of Nb, V, and S, and no P or halogen atom was detected. A quantitative analysis performed with standards gave $Nb_{1.20}V_{0.80}S_5$. The composition of the compound was determined to be $Nb_{1+x}V_{1-x}S_5$ ($x = 0.18$) by a single-crystal X-ray diffraction study. A stoichiometric $NbVS_5$ phase has not been found in subsequent experiments in which various ratios of Nb and V were loaded. Attempts to prepare the $Nb_{1+x}V_{1-x}S_5$ phase without P and/or halide fluxes in our lab have not been successful, and the role of P and halides in this reaction is not yet clear.

Crystallographic Studies. The crystal structure of $Nb_{1+x}V_{1-x}S_5$ was determined by single-crystal X-ray diffraction methods. Preliminary examination and data collection were performed on a Mac Science MXC3 diffractometer equipped with graphite-monochromated Mo Kα radiation ($\lambda(K\alpha_1) = 0.7093$ Å). Cell constants and an orientation matrix were determined from least-squares analysis, using setting angles of 23 reflections in the range $20.0° < 2\theta(\text{Mo K}\alpha) < 28.0°$ that had been automatically centered. The intensities of standard reflections measured every 100 reflections showed no significant deviations during the data collection. Intensity data for the title compound were collected at room temperature with the $\omega-2\theta$ scan technique. Additional crystallographic details are described in Table 1.

The systematic absence ($0k0$, $k = 2n + 1$) is consistent with monoclinic space groups C_2^2-$P2_1$ and C_{2h}^2-$P2_1/m$. The centrosymmetric $P2_1/m$ was assumed, and the satisfactory refinement confirmed the choice of this space group. Initial positions for all atoms of the stoichiometric $NbVS_5$ were obtained by using direct methods of the SHELXS-86 program.[6] The structure was refined by full-matrix least-squares techniques with the use of the SHELXL-97 program.[7] The refinement afforded residuals wR2 = 0.1471, and the conventional R index based on the reflections having $F_o^2 > 2\sigma(F_o^2)$ is 0.0540.

Table 1. Crystal Data and Structure Refinement for $Nb_{1+x}V_{1-x}S_5$ ($x = 0.18$)

fw, amu	152.08
space group	$P2_1/m$ (No. 11)
a, Å	9.881(4)
b, Å	3.329(1)
c, Å	8.775(3)
β,[a] deg	114.82(3)
vol, Å^3	262.0(2)
Z	2
T, K	293(2)
radiation	graphite-monochromated Mo Kα
linear abs coeff, mm^{-1}	5.871
transm factors	0.816−0.918
density (calcd, mg/m^3)	3.956
cryst size, mm^3	0.36 × 0.03 × 0.016
scan type and range, deg	$\omega-2\theta$ and $1.4 + 0.35 \tan\theta$
2θ limits, deg	$3.0 \le 2\theta \le 52.0$
data collected	$\pm h, +k, +l$
no. of unique data with $F_o^2 > 0$	588 [R(int) = 0.0367]
no. of unique data with $F_o^2 > 2\sigma(F_o^2)$	520
no. of refined params	44
wR2 ($F_o^2 > 0$)[b]	0.1171
R1 (on F_o for $F_o^2 > 2\sigma(F_o^2)$)[c]	0.0457
GOF on F^2	1.055
min and max residual e$^-$ density (e/Å^3)	−1.713 and 2.083

[a] α and γ were constrained to be 90° in the refinement of cell constants. [b] $\text{wR2} = [\sum[w(F_o^2 - F_c^2)^2]/\sum[w(F_o^2)^2]]^{1/2}$. [c] $\text{R1} = \sum||F_o| - |F_c||/\sum|F_o|$.

Table 2. Atomic Coordinates, Occupation Factors, and Equivalent Isotropic Displacement Parameters (Å^2 × 10^3) for $Nb_{1+x}V_{1-x}S_5$

atom	x	y	z	sof	U_{eq}[a]
Nb(1)	0.1380(1)	0.25	0.2220(1)	0.59(1)	
M	0.4041(2)	−0.25	0.0578(2)	0.5	13(1)
Nb(2)				0.09(1)	
V(2)				0.41(1)	
S(1)	0.4104(3)	0.25	0.2621(4)	0.5	11(1)
S(2)	0.0198(3)	−0.25	0.3433(4)	0.5	11(1)
S(3)	0.2479(3)	−0.25	0.4577(4)	0.5	12(1)
S(4)	−0.1339(3)	0.25	−0.0080(3)	0.5	7(1)
S(5)	0.3373(3)	−0.75	-0.1581(4)	0.5	11(1)

[a] U_{eq} is defined as one-third of the trace of the orthogonalized $\mathbf{U}_{ij}$ tensor.

The displacement parameters for the V site are significantly smaller that those of other atoms, which implies that this site may be shared by V and Nb atoms. The positional and anisotropic displacement parameters of V and Nb in this site are equated by constraints; the occupation factors of each atom have been freely refined, but their sum is constrained to be constant for the full occupancy of the site (sof = 0.5). No evidence was found for ordering of this site, and thus a statistically disordered structure is assumed. The result of the refinement was improved significantly by introducing disorder in the octahedral site, and the best fit was found when $x = 0.18(2)$. (wR2 = 0.1233, R = 0.0448.) With the composition established, the data were corrected for absorption with the use of the analytical method of Tompa and de Meulenar.[8] All atomic displacement parameters were refined anisotropically.

The final cycle of the refinement afforded residuals wR2 = 0.1171; the conventional R index is 0.0457. The disordered model for the Nb sites was also tested but did not improve the refinement. A difference Fourier synthesis calculated with phases based on the final parameters shows no peak heights greater than 2.083 e/Å^3. No unusual trends were found in the goodness of fit as a function of F_o, $\sin\theta/\lambda$, and Miller indices. Final values of the atomic coordinates and equivalent isotropic displacement parameters are given in Table 2. Anisotropic displacement parameters and complete

(5) $CsNb_2PS_{10}$: space group Pc, $a = 14.030(5)$ Å, $b = 7.552(3)$ Å, $c = 12.971(4)$ Å, $\beta = 95.74(3)°$.
(6) Sheldrick, G. M. *Acta Crystallogr.* **1990**, *A46*, 467−473.
(7) Sheldrick, G. M. *SHELXL97. Program for the Refinement of the Crystal Structures*; University of Göttingen: Göttingen, Germany, 1997.
(8) Meulanaer, J. de; Tompa, H. *Acta Crystallogr.* **1965**, *19*, 1014−1018.

Table 3. Selected Interatomic Distances (Å) and Angles (deg) for $Nb_{1+x}V_{1-x}S_5$[a]

Nb−S(4)#1	2.497(2)	M−S(5)#5	2.327(4)
Nb−S(2)	2.512(2)	M−S(5)	2.397(3)
Nb−S(3)	2.518(2)	M−S(1)	2.428(3)
Nb−S(1)	2.564(3)	M−S(4)#1	2.518(3)
Nb−S(4)	2.597(3)	M−M#5	3.000(3)
Nb−Nb#3	3.3287(13)	M−M#3	3.3287(13)
Nb−Nb#4	3.3287(13)		
S(2)−S(3)	2.046(4)		
S(4)#1−Nb−S(4)#2	83.60(10)	S(5)#5−M−S(5)	101.16(10)
S(4)#1−Nb−S(2)	90.77(8)	S(5)#5−M−S(5)#3	101.16(10)
S(4)#2−Nb−S(2)	153.72(10)	S(5)−M−S(5)#3	87.97(12)
S(4)#1−Nb−S(2)#3	153.72(10)	S(5)#5−M−S(1)	92.12(11)
S(4)#2−Nb−S(2)#3	90.77(8)	S(5)−M−S(1)	166.61(13)
S(2)−Nb−S(2)#3	83.00(10)	S(5)#3−M−S(1)	91.18(8)
S(4)#1−Nb−S(3)#3	157.45(10)	S(5)#5−M−S(1)#4	92.12(11)
S(4)#2−Nb−S(3)#3	92.44(8)	S(5)−M−S(1)#4	91.18(8)
S(2)−Nb−S(3)#3	101.94(9)	S(5)#3−M−S(1)#4	166.61(13)
S(2)#3−Nb−S(3)#3	48.01(10)	S(1)−M−S(1)#4	86.56(12)
S(4)#1−Nb−S(3)	92.44(8)	S(5)#5−M−S(4)#1	168.99(13)
S(4)#2−Nb−S(3)	157.45(10)	S(5)−M−S(4)#1	86.70(10)
S(2)−Nb−S(3)	48.01(10)	S(5)#3−M−S(4)#1	86.70(10)
S(2)#3−Nb−S(3)	101.94(9)	S(1)−M−S(4)#1	79.92(10)
S(3)#3−Nb−S(3)	82.74(10)	S(1)#4−M−S(4)#1	79.92(10)
S(4)#1−Nb−S(1)	77.74(9)		
S(4)#2−Nb−S(1)	77.74(9)		
S(2)−Nb−S(1)	126.16(8)		
S(2)#3−Nb−S(1)	126.16(8)		
S(3)#3−Nb−S(1)	79.72(9)		
S(3)−Nb−S(1)	79.72(9)		
S(4)#1−Nb−S(4)	74.37(9)		
S(4)#2−Nb−S(4)	74.37(9)		
S(2)−Nb−S(4)	79.38(9)		
S(2)#3−Nb−S(4)	79.38(9)		
S(3)#3−Nb−S(4)	125.96(8)		
S(3)−Nb−S(4)	125.96(8)		
S(1)−Nb−S(4)	142.27(10)		

[a] Symmetry transformations used to generate equivalent atoms: #1−*x*, −*y*, −*z*; #2−*x*, −*y*+1, −*z*; #3 *x*, *y*+1, *z*; #4 *x*, *y*−1, *z*; #5−*x*+1, −*y*−1, −*z*.

tabulations on the X-ray studies can be found in CIF format in the Supporting Information.

Results and Discussion

Crystal Structure. Selected interatomic distances and angles for $Nb_{1+x}V_{1-x}S_5$ are given in Table 3. A view down the **b**-axis (Figure 1) clearly shows the layered nature of the structure. Figure 2 shows that an individual layer is composed of two unique chains of face-sharing Nb-centered bicapped trigonal prisms and edge-sharing M-centered octahedra (M = Nb or V). This compound is isostructural with $Fe_{1+x}Nb_{3-x}Se_{10}$, and detailed descriptions of this structural type have been given previously.[9]

The Nb atom is surrounded by six S atoms in trigonal prismatic fashion. Atoms S(2), S(3), and S(4) form a triangle that is isosceles rather than equilateral, the S(2)−S(3) distance (2.046(4) Å) being much shorter than the other two (>3.0 Å). This short S(2)−S(3) separation is consistent with a typical $(S-S)^{2-}$ pair.[10] The Nb atoms are further coordinated by two additional S atoms that cap two of the rectangular faces of the trigonal prism. The Nb−S distances, ranging from 2.497(2) to 2.597(3) Å, are in agreement with

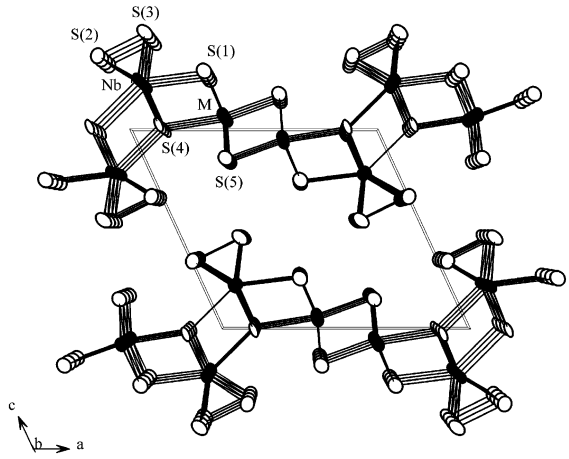

Figure 1. View of $Nb_{1+x}V_{1-x}S_5$ down the **b**-axis (needle axis) showing the stacking of the layers. Displacement ellipsoids are drawn at the 80% probability level. The M site is occupied by statistically disordered Nb (18%) and V (82%) atoms.

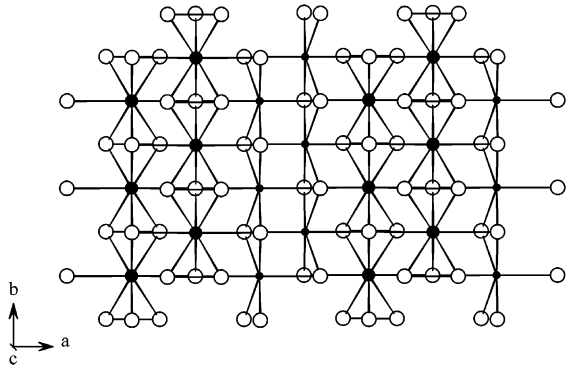

Figure 2. View of $Nb_{1+x}V_{1-x}S_5$ down the **c**-axis (needle axis) showing an individual layer and the coordination around the Nb and M atoms. Large filled circles are Nb atoms, small filled circles are M atoms, and open circles are S atoms.

the Nb−S distances found in related phases.[11] Longer Nb−S distances are observed for the capping S atoms. The Nb-centered bicapped trigonal prisms share their triangular faces to form a one-dimensional chain, $^1_\infty[NbS_5]$, along the direction of the **b**-axis. Two Nb chains are linked together by sharing two S(4) atoms to form a double bicapped trigonal prismatic chain, $^1_\infty[Nb_2S_8]$. The same geometry can be found in other group 5 metal chalcogenides such as $NbSe_3$ (the isosceles type I and III chains)[12] and Ta_2MSe_7 (M = Ni, Pd, and Pt).[13] However, the Nb-centered trigonal prism found in $Nb_{1+x}V_{1-x}S_5$ is different from that of NbS_3.[14] The Nb atoms associate in pairs in NbS_3, with Nb···Nb interactions alternating in the sequence of one short (3.037(3) Å) and one long distance (3.693(3) Å). The Nb···Nb separation

(9) Meerschaut, A.; Gressier, P.; Guemas, L.; Rouxel, J. *Mater. Res. Bull.* **1981**, 1035−1040.

(10) Kim, C.; Yun, H. *Acta Crystallogr.* **2002**, *C58*, i53−i54.

(11) (a) Do, J.; Yun, H. *Inorg. Chem.* **1996**, *35*, 3729−3730. (b) Evain, M.; Brec, R.; Whangbo, M. H. *J. Solid State Chem.* **1987**, *71*, 244−262.

(12) (a) Meerschaut, A.; Rouxel, J. *J. Less Common Met.* **1975**, *39*, 197−203. (b) Hoffmann, R.; Shaik, S.; Scott, J. C.; Whangbo, M. H.; Foshee, M. J. *J. Solid State Chem.* **1980**, *34*, 263−269. (c) Canadell, E.; Rachidi, I. E.-I.; Pouget, J. P.; Gressier, P.; Meerschaut, A.; Rouxel, J.; Jung. D.; Evain, M.; Whangbo, M. H. *Inorg. Chem.* **1990**, *29*, 1401−1407.

(13) Sunshine, S.; Ibers, J. *Inorg. Chem.* **1986**, *25*, 4355−4358.

(14) Rijnsdorp, J.; Jellinek, F. *J. Solid State Chem.* **1978**, *25*, 325−328.

in $Nb_{1+x}V_{1-x}S_5$ (3.329(1) Å) is close to the average Nb···Nb separations in NbS_3 (3.383 Å).

The M site occupied by 18% of Nb and 82% of V is surrounded by six S atoms in distorted octahedral fashion. These octahedra then share their edges through atoms S(1) and S(5) to form a one-dimensional chain, $^1_\infty[MS_4]$. Again, two octahedral chains are bound by sharing two S(5) atoms and thus form a double octahedral M chain, $^1_\infty[M_2S_6]$. In spite of the partial occupation of Nb, the M−S distances are in good agreement with that calculated from crystal radii typical for V and S atoms in sulfide structure, except for the M−S(4) distance (2.518(3) Å). This double octahedral chain can be found in many other compounds, such as Ta_2NiS_5.[15] These structural units often allow significant interchain zigzag metal−metal interactions, and an intermediate M···M separation (3.000(3) Å) is found in $Nb_{1+x}V_{1-x}S_5$. This is much shorter than the interchain Ta···Ta distance (>3.7 Å) in Ta_2NiS_5,[15] even if account is taken of the different ionic radii of each metal atom. The intrachain M···M distance is the same as the repeating unit along the **b**-axis (3.329(1) Å) and significantly longer than the interchain M···M distance.

Both metal and S atoms in double Nb and M chains are related by the 2_1 screw axial symmetry. These double Nb and M chains are condensed together through S(1) and S(4), and a quadruple $^1_\infty[Nb_2M_2S_{12}]$ chain is completed. Finally, these $^1_\infty[Nb_2M_2S_{12}]$ chains are connected along the **a**-axis to form a two-dimensional layer, $^2_\infty[NbMS_5]$. These layers then stack on top of each other to form the three-dimensional structure with an undulating van der Waals gap shown in Figure 1. There is no bonding interaction, only van der Waals forces, between the layers.

The $MM'Te_5$ (M = Nb,Ta; M′ = Ni, Pd, Pt) phases also have a layered structure consisting of M-centered bicapped trigonal prismatic chains and M′-centered octahedral chains.[16] In this structural type, however, two kinds of single chains alternate to form the layer, instead of the double chains found in $Nb_{1+x}V_{1-x}S_5$. In addition, the short sides of the triangular face of the trigonal prism ($d_{Te\cdots Te}$ > 3.1 Å) in the $MM'Te_5$ phases are significantly longer than the distance of 2.92 Å expected for a $(Te-Te)^{2-}$ bond.

Band Structure. In order to understand the electronic structure of this compound, we have performed band structure calculations. Because the Nb concentration in the octahedral chain is small, we assume initially that perturbations caused by Nb atoms in this chain are not significant. In this approximation, band structure calculations on the stoichiometric $NbVS_5$ were first carried out. We later turn to the actual $Nb_{1+x}V_{1-x}S_5$ structure. In the actual system, the V and Nb atoms in the octahedral chain occur in an approximately 5:1 ratio and are believed to be randomly distributed. Electronic structure calculation on a disordered structure is difficult. In our work we will study the effect of the disorder by considering modeled ordered structures. There are a number of differently ordered arrangements, and we used the simplest ordered model to study the effects of the disorder in the octahedral chain. The model chosen triples the **b**-axis and replaces one out of six V atoms with a Nb atom. The new extended unit cell in this model contains 7 Nb atoms, 5 V atoms, and 30 S atoms. Details of the calculations are described in the Appendix.

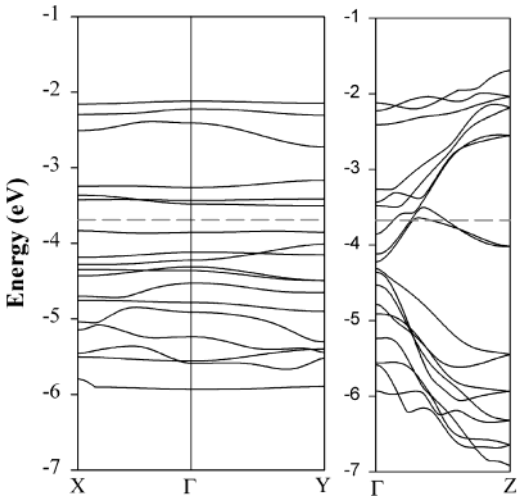

Figure 3. The band structure of $NbVS_5$ calculated by DFT. The dashed line refers to the Fermi level. The Γ, *X*, *Y*, and *Z* labels refer to the reduced wave vectors (0, 0, 0), (0.5, 0, 0), (0, 0.5, 0), and (0, 0, 0.5), respectively. The coordinate system is defined in structures **1** and **5**.

We display the density functional theory (DFT)-calculated electronic structure of the hypothetical, stoichiometric $NbVS_5$ along selected high-symmetry lines within the first Brillouin zone of the lattice in Figure 3.

We mention here that our desire to have the d orbitals of Nb and V simply expressed led us to a reorientation of the absolute *x*, *y*, *z* coordinate system relative to the crystal **a**, **b**, **c** direction. In order to keep the classical form of the z^2 and $x^2 - y^2$ orbitals, the *z* direction has been assigned to be parallel to the chain axis (**b**-axis). Note that the new coordinate system for the band structure analysis is defined in the structure **1** and **5**. As expected from related compounds, such as $NbSe_3$[12b] and $Fe_{1+x}Nb_{3-x}Se_{10}$,[4b] the dispersion is significant only along the direction of the chains and the bands are flat perpendicular to the chain axis, indicating the one-dimensional nature of the compound. As shown in this figure, the Fermi level cuts through bands along Γ → *Z* (i.e., along the **b***-axis) but not along the symmetry lines Γ → *X* and Γ → *Y*. Therefore the system should be metallic along the **b**-axis, in agreement with four-probe conductivity data measured along the needle axis of the crystal.[17] Because of the screw axis along **b**, all bands are doubly degenerate at *Z*.

An extended Hückel (EH) method[18] analysis was carried out to understand the nature of interactions between chains and overlapping among metals and sulfur atoms. The band

(15) Sunshine, S.; Ibers, J. *Inorg. Chem.* **1985**, *24*, 3611−3614.
(16) (a) Liimatta, E.; Ibers, J. *J. Solid State Chem.* **1987**, *71*, 384−389. (b) Liimatta, E.; Ibers, J. *J. Solid State Chem.* **1988**, *77*, 141−147. (c) Liimatta, E.; Ibers, J. *J. Solid State Chem.* **1989**, *78*, 7−16. (d) Mar, A.; Ibers, J. *J. Solid State Chem.* **1991**, *92*, 352−361.
(17) Electronic conductivity was measured by the ordinary four-probe method using a Keithley 181 nanovoltmeter along the needle axis of the crystal. $Nb_{1+x}V_{1-x}S_5$ ($x = 0.18$) is metallic at room temperature; it undergoes a transition below 50 K. Studies on the conductivity are currently underway.
(18) Hoffmann, R. *J. Chem. Phys.* **1963**, *39*, 1397−1412.

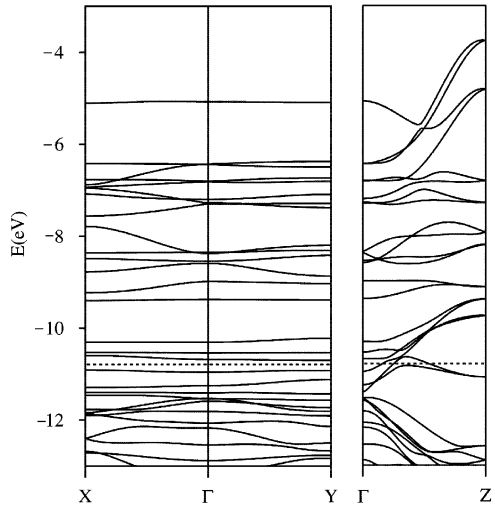

Figure 4. The band structure of $NbVS_5$ calculated by EHT. The dashed line refers to the Fermi level.

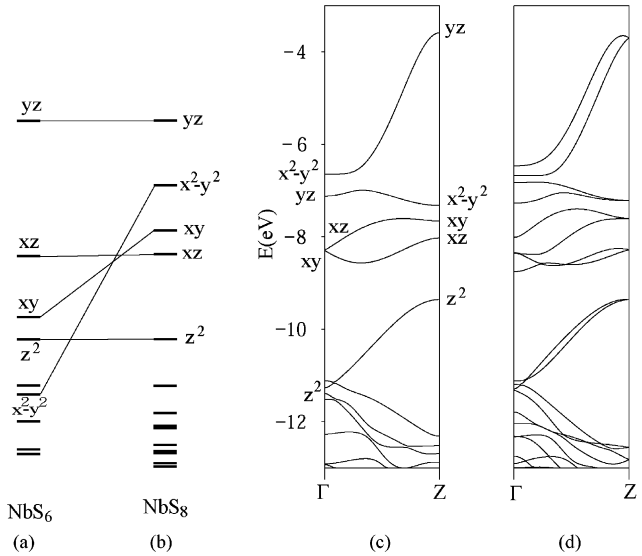

Figure 5. The MO diagrams of monomeric NbS_6 (a) and NbS_8 (b). The band structures for a single $^1_\infty[NbS_5]$ chain (c) and a double $^1_\infty[Nb_2S_8]$ chain (d).

structure of $NbVS_5$ calculated with EHT is given in Figure 4. The general features of the bands around the Fermi level calculated by the better DFT method remain intact in the EHT computation.

In approaching an understanding of the three-dimensional $NbVS_5$, we need to become familiar with the electronic structure of the basic building units, the bicapped isosceles trigonal prismatic NbS_8 and the VS_6 octahedron. The molecular orbital (MO) diagram for the hypothetical NbS_6 (**1**) complex in approximate C_{2v} geometry is shown in Figure 5a. In NbS_6, the Nb 4d orbitals split into five separate levels, in a typical trigonal prism crystal field.[12b]

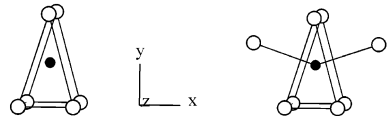

Structure **1** Structure **2**

The perturbation resulting from the S atoms of a neighboring chain can be understood by approaching two capping S atoms to the Nb trigonal prism (NbS_8, **2**); the MO diagram is given in Figure 5b. The $x^2 - y^2$ and xy orbitals of the Nb atom are extended toward the capping S atoms, while this is not the case with the z^2 orbital. Therefore, the $x^2 - y^2$ and xy orbitals interact more effectively with the capping S atoms, and are raised with respect to the z^2 level (relative to the six-coordinate complex). The S−S bonding (σ) and antibonding (σ^*, not shown in the figure) levels are positioned below and above the Nb d block orbitals, respectively.

The effect of translational symmetry in one dimension along the chain axis can be approached through the band structure of the bicapped trigonal prismatic chain ($^1_\infty[NbS_5]$, **3**), shown in Figure 5c. The d-block orbitals of the NbS_8

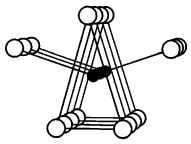

Structure **3**

molecular unit spread out into bands of substantial width (up to ∼3 eV). If contributions from intrachain Nb···Nb interactions were dominant, the most antibonding combination of the yz level would be found at the zone center, Γ. However, this band runs up along $\Gamma \rightarrow Z$; the interaction responsible for this is primarily Nb−S coupling; direct overlap of the metal d orbitals is small at this long Nb···Nb separation (3.329(1) Å). As was pointed out by Whangbo et al., in the analysis of MO of the isostructural $NbSe_8$ complex[1a], the $x^2 - y^2$ and xy bands are removed from the region of the z^2 band (where the Fermi level is) because of the capping S atoms from neighboring chains. Therefore, the z^2 band of Nb is mainly responsible for the electrical conduction of the trigonal prismatic chain, and this is induced by the Nb-capping S interactions. At the same time, the p block bands from the in-plane p_x and p_y orbitals of capping S atoms from the nearest-neighbor chains are lowered by these Nb−S bonding interactions. This stabilization is one of the driving forces for the one-dimensional chains to link together to form the two-dimensional layer.

The band structure of the double Nb chain ($^1_\infty[Nb_2S_8]$, **4**) is shown in Figure 5d. The bands are generally doubled, as

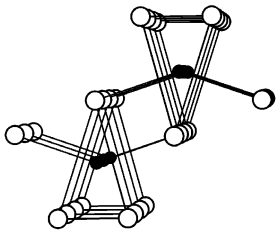

Structure **4**

expected, the perturbation varying with the spatial extent of the metal d orbitals. For instance, the perturbation on the yz band is much larger than that of the z^2 band. This could be

explained by the fact that the z^2 orbital points along the chain axis, whereas the *yz* orbital is pointed toward the other chain.

We now turn to the V substructure. The coordination around the V atom can be described as a slightly distorted octahedron. The MO calculated in a model VS_6 complex (**5** in the geometry cut of the solid) shows the typical three-below-two pattern (Figure 6a) of this coordination. The band

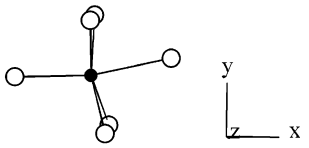

Structure **5**

structure of the V octahedral chain ($^1_\infty[VS_4]$, **6**) is given in Figure 6b. The d block orbitals of the molecular VS_6 unit

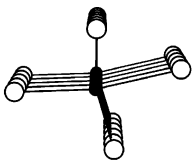

Structure **6**

spread out into bands of width up to 2.5 eV. A gap of ~2.5 eV between e_g ($x^2 - y^2$, *yz*) and t_{2g} (*xy*, *xz*, z^2) bands is easily recognized. The band mainly derived from the *yz* orbital is more dispersive than the others, because the *yz* orbital of V can interact more effectively with p_x and p_y orbitals of S(1) and S(2), compared to the other V d orbitals.

The band structure of the double V chain ($^1_\infty[V_2S_6]$, **7**) is given in Figure 6c. Again, the bands are generally doubled.

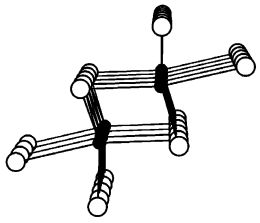

Structure **7**

However, in this double octahedral chain there is an intermediate strength interchain V···V interaction ($d_{V\cdots V}$ = 3.000(3) Å), propagating in a zigzag fashion parallel to the **b**-axis. Consequently, we expect some band dispersion along the line $\Gamma \rightarrow Z$. As can be seen from comparing Figures 5d and 6c, the *xz* and *xy* bands in the V chain become more seriously perturbed on doubling, compared to the corresponding Nb d bands.

We have investigated the electronic structures of the discrete mononuclear complexes and one-dimensional chains in order to understand the nature of interactions among atoms and between chains. This compound has a layered structure, and the layer is composed of the double Nb chain and the double V chain parallel to the **b**-axis. These chains are repeated along the **a**-axis to complete the layer. Therefore, the effect of translation of each chain along the **a**-axis can be understood through the band structure of the isolated two-

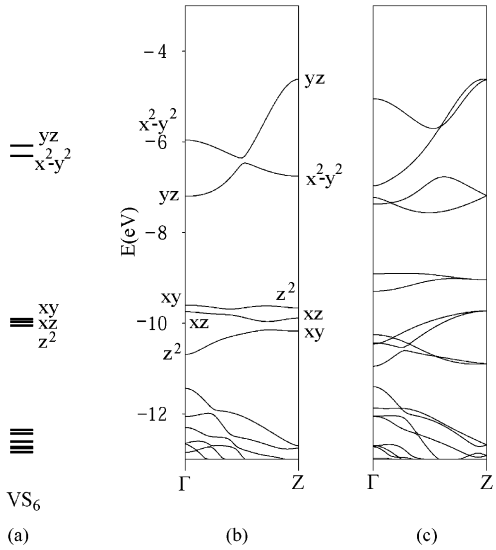

Figure 6. The MO diagram of monomeric VS_6 (a). The band structures for a single $^1_\infty[VS_4]$ chain (b) and a double $^1_\infty[V_2S_6]$ chain (c).

dimensional slab, $^2_\infty[NbVS_5]$ parallel to the **ab** plane. As expected, the band structure along the line $\Gamma \rightarrow Z$ of the two-dimensional layer can be generated by superimposing those of the $^2_\infty[Nb_2S_8]$ and $^2_\infty[V_2S_6]$ chains. We also find that the three-dimensional band structure is similar to that of the single layer. Interlayer orbital overlap interactions across the van der Waals gap are clearly unimportant. This derives from the large S···S separations ($d_{S\cdots S}$ > 3.2 Å) across the layers. However, this may not be the same for the more polarizable chalcogens, especially for Te. In the $MM'Te_5$ (M = Nb, Ta; M′ = Ni, Pd, Pt) phases, for example, the three-dimensional band structure is not just the superposition of that of the single layer, and some bands become dispersive considerably upon the interlayer interaction. These interactions have been reported to play a crucial role in the electrical properties, by inducing electron transfer from the Te atoms to metals.[19]

The total and partial DOS for $NbVS_5$ is shown in Figure 7. The sulfur orbitals are in the lower part of the plot (below −11.4 eV), and contributions derived mainly from S(2)−S(3) interactions are found below −12 eV. The bands that form the middle region, extending over the range −3.5 to −11.4 eV, are composed of the metal d orbitals (Nb 4d and V 3d) and S 3p orbitals. Contributions to the DOS of each element are illustrated on the right-hand side of Figure 7. The Nb 4d and V 3d bands spread over about 7 eV. The p states of Nb and V lie higher in energy by several electronvolts. Because the metal d and S p bands are rather wide and overlap considerably, strong covalent bonding between metals and sulfur atoms is expected. The position of the Fermi level at −10.78 eV, at a nonzero point of the DOS, indicates that $NbVS_5$ should be metallic. Since the DOS for the Nb atom at the Fermi level is small, the conductivity occurs mainly through carriers in the V t_{2g} and S 3p orbitals.

(19) (a) Alemany, P.; Canadell, E. *Eur. J. Inorg. Chem.* **1999**, 1701−1706. (b) Halet, J.; Hoffmann, R.; Tremel, W.; Liimatta, E.; Ibers, J. *Chem. Mater.* **1989**, *1*, 451−459.

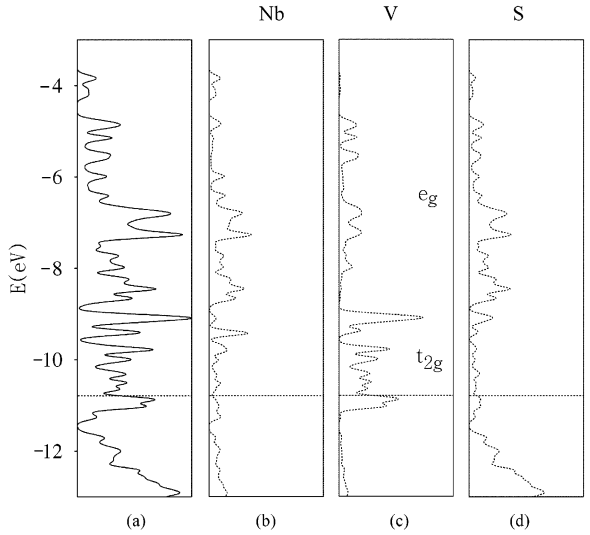

Figure 7. Density of states (DOS) curves for $NbVS_5$: (a) total DOS; (b) Nb contribution to DOS; (c) V contribution to DOS; (d) S contribution to DOS.

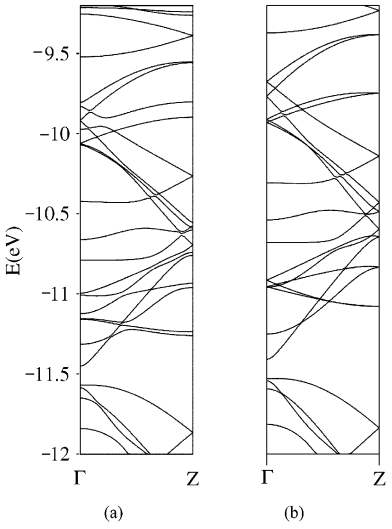

Figure 8. The band structure for (a) the ordered model, $Nb_{1+x}V_{1-x}S_5$ ($x = 0.18$), and (b) the stoichiometric $NbVS_5$ with tripled unit cell discussed in the text.

Whangbo et al. have carried out band structure calculations on the $Fe_{1+x}Nb_{3-x}Se_{10}$ phase and reported that the electrons responsible for conduction reside primarily on the prismatic chains.[4b] This is because the band near the Fermi level arises overwhelmingly from the z^2 orbital of the Nb atoms in the trigonal prismatic chains. This cannot be the same even if $Fe_{1+x}Nb_{3-x}Se_{10}$ is isostructural with $NbVS_5$. The energy level of V 3d orbitals (H_{ii}(V 3d) $= -11.0$ eV) is higher than that of the Nb 4d orbitals ($H_{ii} = -12.10$ eV) whereas Fe 3d orbitals ($H_{ii} = -12.6$ eV) is below the Nb 4d orbitals. As a result, bands of primarily Fe 3d orbital character (in $Fe_{1+x}Nb_{3-x}Se_{10}$) lie well below the Fermi level in the band structure. However, bands arising from the V 3d orbitals, especially the t_{2g} levels in $NbVS_5$, occur around the Fermi level. As a result, contributions of the electrons in the V t_{2g} orbitals to the transport properties of the material should be significant.

The formal charge assignment $[(NbV)^{8+}][S_2^{2-}][S^{2-}]_3$ is consistent with the structure. The S(2)−S(3) distance is typical of the $(S-S)^{2-}$ pair; a -2 oxidation number can be assigned to all the other three S atoms. However, it is difficult to describe the oxidation state of each metal ion, not only because of the disordered nature of the compound, but because of the superposition of d bands of each metal ion around the Fermi level. To get a clue to the oxidation state of Nb and V ions, contributions of each metal atom for the three low-lying bands near the Fermi level were analyzed. Some care must be taken in such an analysis. For example, the atomic Mulliken charges would not correlate with formal oxidation states. Instead we use the following procedure. As we have shown in Figures 5 and 6, the actual bands may be assigned to specific Nb and V d orbitals. We therefore need only to calculate the occupation of these bands to deduce the correct formal oxidation state. In this, we are abetted by the separable nature of the Nb and V orbitals discussed above. Only in the case of the partially occupied bands must some additional care be taken. These bands near Γ are predominantly Nb-like, while those near *Z* display more V character. To assign these bands, the occupancies of metal atom were calculated by integrating the squares of the orbital coefficients of metal orbitals at various *k*-points along Γ → *Z*. The relative occupancies of the d levels of Nb and V calculated in this way were 0.55 and 1.45, respectively, and this can be converted to $Nb^{4.45+}$ and $V^{3.55+}$. If the oxidation state of +4.45 is also assigned to the Nb atom in the octahedral chain, the oxidation number of the V ions should be +3.37. These numbers are of course approximate, as may be expected with both the concept of oxidation state and the level of calculation.

So far we have discussed a hypothetical ordered phase $NbVS_5$. As we discussed earlier, structural refinement on the disordered $Nb_{1+x}V_{1-x}S_5$ phase carried out by varying x gives the best fit for $x = 0.18$, and this result is supported by the quantitative elemental analysis. We need to approach the electronic structure of the disordered real material. This we do by a calculation for an assumed superstructure. Our model structure for the hypothetical ordered $Nb_{1+x}V_{1-x}S_5$ ($x = 0.18$) can be generated by tripling the **b**-axis and substituting one of the six V atoms for a Nb atom in the double octahedral chain. The d band dispersion spanning the range 0 to **b***/2 is folded into three segments in the region 0 to **b***/6 upon tripling the **b**-axis. For comparison, the band dispersion diagram of the ordered model $Nb_{1+x}V_{1-x}S_5$ is given in Figure 8a along with that of the stoichiometric $NbVS_5$ with tripled unit cell (Figure 8b). The electronic bands of the trigonal prismatic chain remain intact except for the folding.[20] However, the band structure of the octahedral chain is obviously perturbed slightly. Bands from the octahedral chain lose degeneracy at Γ and *Z* because the crystallographic 2_1 screw axial symmetry is violated by the Nb atom in the chain. Except for this minor perturbation, the electronic structure of the ordered $Nb_{1+x}V_{1-x}S_5$ phase still keeps the key features of those of the stoichiometric $NbVS_5$.

(20) Hoffmann, R. *Solids and Surfaces: A Chemist's View of Bonding in Extended Structures*; Wiley-VCH: New York, 1988.

Appendix

DFT Calculations. Density functional (DF) calculations were performed with the CRYSTAL98 software package,[21] which is based on the use of periodic ab initio LCAO (linear combination of atomic orbitals). We employed the local density approximation (LDA) to DFT using Dirac−Slater exchange[22] and Perdew−Zunger correlation functionals.[23] The reciprocal space integration was performed by sampling the irreducible part of the first Brillouin zone at a regular set of 68 *k*-points defined by the shrinking factors IS = 6, ISP = 12.

Bloch functions are constructed from basis functions localized on atoms; such functions, in turn, are linear combination of Gaussian type orbitals (GTO). In this calculation, effective core potentials (ECP) basis sets were employed. The basis sets used were [HAYWSC]-31(31d)G for Nb, [HAYWSC]-41(31d)G for V, and [DURAND]-31G* for S.[24] For Nb and V basis sets, the valence shell orbital exponents and contraction coefficients were reoptimized from Nb^{5+} and V^{2+} basis sets,[25,26] to satisfy formal charge conditions of Nb^{4+} and V^{4+}. The optimizations were obtained by minimizing the calculated energy of crystal structures of NbS_2 and VS_2 using LoptCG, a ksh-script that performs numerical gradient energy optimizations.[27]

EHT Calculations. Band structure calculations were performed with an extended Hückel type Hamiltonian (YAeHMOP).[28] Various values of the ionization potential, H_{ii}, of the S 3p orbitals were tested. A choice of H_{ii}(S 3p) = −13.3 eV gave band structures close to those of DFT calculations and thus was selected for the EHT analysis. The atomic parameters used in the present study are listed in Table 4.

Table 4. Extended Hückel Parameters

atom	orbital	H_{ii} (eV)	ζ_{11}	c_1	ζ_{12}	c_2
Nb	5s	−10.10	1.89			
	5p	−6.86	1.85			
	4d	−12.10	4.08	0.6401	1.64	0.5516
V	4s	−8.81	1.30			
	4p	−5.52	1.30			
	3d	−11.0	4.75	0.4755	1.70	0.7052
S	3s	−20.0	2.122			
	3p	−13.3	1.827			

Acknowledgment. This research was supported by the Korean Science and Engineering Foundation (KOSEF 2000-1-12200-002-3). Work in Cornel University was supported by the NSF (Grant DMR-0073587).

Supporting Information Available: One X-ray crystallographic file in CIF format. This material is available free of charge via the Internet at http://pubs.acs.org.

IC0205334

(21) Dovesi, R.; Roetti, C.; Causa, M.; Harrison, N. M.; Orlando, R.; Apra, E. *CRYSTAL98 User's Manual*; University of Torino, Torino, 1996
(22) Dirac, P. A. M. *Proc. Cambridge Philos. Soc.* **1930**, *26*, 376−385.
(23) Perdew, J. P.; Zunger, A. *Phys. Rev.* **1981**, *B16*, 5048−5079.
(24) Ouazzani, T.; Lichanot, A.; Pisani, C.; Roetti, C. *J. Phys. Chem. Solids* **1993**, *54*, 1603−1611.
(25) Dall'Olio, S.; Dovesi. R.; Resta, R. *Phys. Rev.* **1997**, *B52*, 10105−10114.
(26) Mackrodt, W. C.; Harrison, N. M.; Saunders: V. R.; Allan, N. L.; Towler, M. D.; Aprà, E.; Dovesi, R. *Philos. Mag.* **1993**, *A68*, 653−666.
(27) LoptCG written and developed by C. M. Zicovich-Wilson, Instituto de Tecnología Química, UPC-CSIC, Spain, 1988.
(28) Landrum, G. A. The *YAeHMOP* extended Hückel package available on the WWW at URL http://yaehmop.sourceforge.net/.